



A Journal of the Gesellschaft Deutscher Chemiker

Angewandte Chemie

GDCh

International Edition

www.angewandte.org

Accepted Article

Title: Confinement-Driven Enantioselectivity in 3D Porous Chiral Covalent Organic Frameworks

Authors: Bang Hou, Shi Yang, Kuiwei Yang, Xing Han, Xianhui Tang, Yan Liu, Jianwen Jiang, and Yong Cui

This manuscript has been accepted after peer review and appears as an Accepted Article online prior to editing, proofing, and formal publication of the final Version of Record (VoR). This work is currently citable by using the Digital Object Identifier (DOI) given below. The VoR will be published online in Early View as soon as possible and may be different to this Accepted Article as a result of editing. Readers should obtain the VoR from the journal website shown below when it is published to ensure accuracy of information. The authors are responsible for the content of this Accepted Article.

To be cited as: *Angew. Chem. Int. Ed.* 10.1002/anie.202013926

Link to VoR: <https://doi.org/10.1002/anie.202013926>

RESEARCH ARTICLE

Confinement-Driven Enantioselectivity in 3D Porous Chiral Covalent Organic Frameworks

Bang Hou[†], Shi Yang[†], Kuiwei Yang, Xing Han, Xianhui Tang, Yan Liu,^{*} Jianwen Jiang^{*} and Yong Cui^{*}[*] B. Hou,^[†] S. Yang,^[†] X. Han, X. Tang, Prof. Y. Liu, Prof. Y. Cui

School of Chemistry and Chemical Engineering, Frontiers Science Center for Transformative Molecules and State Key Laboratory of Metal Matrix Composites

Shanghai Jiao Tong University, Shanghai 200240 (China)

E-mail: liuy@sztu.edu.cn, yongcui@sztu.edu.cn.

K. Yang, Prof. J. Jiang

Department of Chemical and Biomolecular Engineering

National University of Singapore, 117576 Singapore

Email: chejj@nus.edu.sg

[†] These authors contributed equally to this work.

Supporting information for this article is given via a link at the end of the document.

Abstract: Covalent organic frameworks (COFs) show great potential in heterogeneous catalysis, but the confinement effect of frameworks on molecular catalysts has yet to be explored. Here we demonstrate the utilization of 3D COFs with well-defined porous channels capable of inducing chiral molecular catalysts from non-enantioselective to highly enantioselective in catalyzing organic transformations, sharply different from the typical methods for tailoring enantioselectivities by varying steric and electronic properties of molecular catalysts. By condensations of a tetrahedral tetraamine and two linear dialdehydes derived from enantiopure 1,1'-binaphthol (BINOL), two chiral 3D COFs with a 9-fold or 11-fold interpenetrated diamondoid framework are prepared. Obviously enhanced Brønsted acidity was observed for the chiral BINOL units that are uniformly distributed within the tubular channels compared to the non-immobilized acids. This facilitates the Brønsted acid catalysis of cyclocondensation of aldehydes and anthranilamides to produce 2,3-dihydroquinazolinones. While homogeneous BINOL controls display no enantioselectivity and/or low activity, constraint of their conformations in CCOFs leads to up to 91% isolated yield with 97% ee. DFT calculations show COF catalyst provide preferential secondary interactions between the substrate and framework to induce enantioselectivities that are not achievable in homogeneous systems.

Introduction

Since its first reported use in asymmetric catalysis by Noyori in 1979, optically pure 1,1'-binaphthol (BINOL), together with other axially chiral biaryldiols, has become one of the most widely used ligands/catalysts^[1,2] and also an attractive platform for chiral recognition and optics.^[3,4] Remarkably, in the past decades, a variety of effective catalysts with the BINOL scaffold have been designed and utilized in numerous asymmetric catalytic organic transformations, especially with the 3,3'-functionalized BINOL derivatives.^[5] In general, the enantioselectivity of reactions is heavily dependent on the steric and electronic properties of substituents in the 3,3'-positions of the BINOL rings, which have a significant effect on substrate activation and structures of transition states and intermediates.^[1] So, exploitation of a new

methodology for the generation and enhancement of BINOL and its derivatives is of great importance in asymmetric catalysis. Unfunctionalized BINOL and its derivatives, an important class of moderate Brønsted acids,^[6] can only promote limited number of asymmetric transformations to produce satisfactory enantioselectivities.^[7] Here we demonstrated that 3D covalent organic frameworks (COFs) can be utilized as an attractive platform to manipulate enantioselectivities of molecular catalysts, which are typically tailored by varying steric and electronic properties of molecular catalysts.^[8]

COFs are a class of network solids constructed by organic molecules through strong covalent bonds in a process named reticular synthesis.^[9] An outstanding feature of COF chemistry is that their robust porosity, stability, and chemical functionality can be controlled by the judicious selection of organic building blocks.^[10] This characteristic has paved the way for their use in diverse applications, including gas separation and storage,^[11] sensing,^[12] catalysis,^[13] and drug release.^[14] Importantly, by condensation of chiral and achiral monomers, a few chiral COFs (CCOFs) can be prepared for enantioselective processes.^[15-17] In particular, we and others have shown that well-defined homogeneous (pre)catalysts can be incorporated into COFs in a systematic fashion to generate single site heterogeneous catalysts with activities and selectivities rivaling those of their homogeneous analogs.^[17] Nevertheless, examples of enantioselective reactions catalyzed by COFs are still very limited and the confinement effect of frameworks on molecular catalysts has yet to be explored.^[18] In this work, we reported that incorporating non-enantioselective BINOLs into conformationally rigid pores of 3D COFs can induce highly enantioselectivity in the catalytic synthesis of the practically important dihydroquinazolinones from aldehydes and anthranilamides.^[19] To this end, chiral linker 6,6'-dichloro-2,2'-dihydroxy-1,1'-binaphthyl-4,4'-dialdehyde (**BDA**) and 6,6'-dichloro-4'-(4-formylphenyl)-2,2'-dihydroxy-1,1'-binaphthyl-4-aldehyde (**BPDA**), each of which contains the dialdehyde primary functionality and chiral 2,2'-dihydroxy secondary functionality, was chosen and synthesized. By imine condensations of the chiral monomers and tetra(*p*-aminophenyl)methane (**TAM**), a pair of 3D BINOL-based CCOFs were prepared (Scheme 1). Crystal structures of the as-

RESEARCH ARTICLE

Scheme 1. Synthesis of the Two 3D CCOFs.

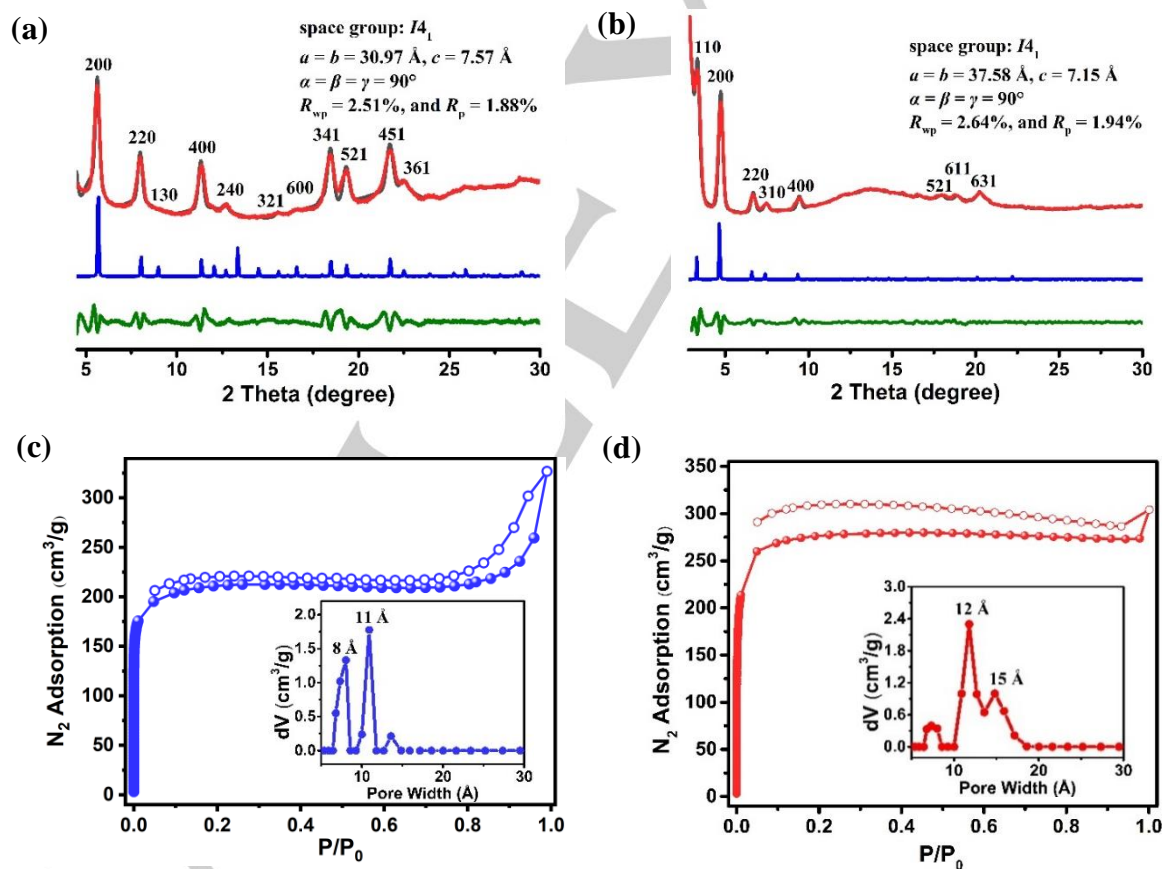
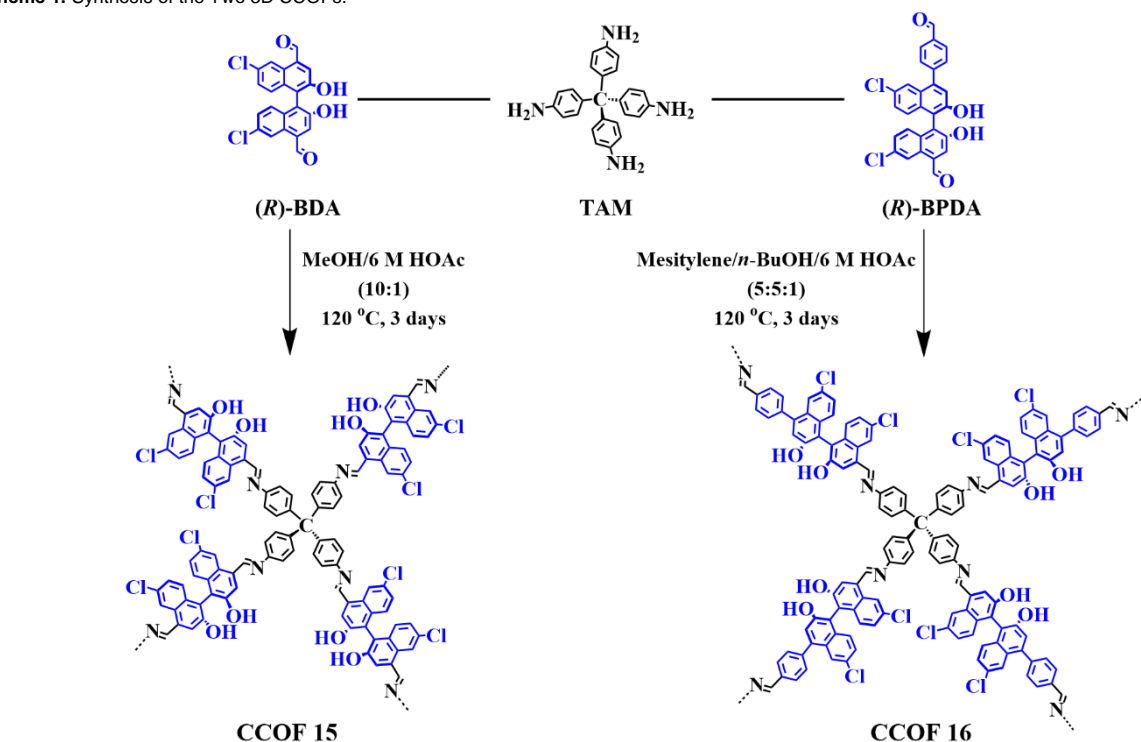


Figure 1. PXRD patterns of a) CCOF 15 and b) CCOF 16 with the experimental profiles in red, Pawley refined in black, calculated in blue, and the difference between the experimental and refined PXRD patterns in dark green. N_2 adsorption-desorption isotherms (77 K) and pore size distribution profiles (insert) of c) CCOF 15 and d) CCOF 16.

RESEARCH ARTICLE

prepared CCOFs were determined by powder X-ray diffraction and modeling studies, as well as pore size distribution analysis. The two isostructural COFs adopt a 9-fold and 11-fold interpenetrated diamondoid open framework with about 8 and 11 Å wide tubular channels, respectively. All BINOL hydroxyls in the frameworks are periodically aligned within the channels can be used as efficient heterogeneous catalysts for the cyclocondensation of aldehydes and anthranilamides with high enantioselectivity. DFT calculations suggest that the 3D porous framework offers a chiral confined microenvironment that dictates enantioselectivity of the catalysis.

Results and Discussion

As shown in Scheme 1, CCOFs **15** and **16** were synthesized by solvothermal reactions of enantiopure (*R*)-**BDA** (0.063 mmol) or (*R*)-**BPDA** (0.063 mmol) and **TAM** (0.032 mmol) in 1.0 mL methanol or 1.0 mL *n*-butanol and mesitylene (1:1 v/v) in the presence of acetic acid (6 M, 0.1 mL) at 120 °C for 3 days, which afforded yellow or orange polycrystalline solids in 86% and 79% yields, respectively.

In the FT-IR spectra of **15** and **16**, the characteristic C=O stretching bands (1680 and 1686 cm⁻¹) were barely present, indicative of the consumption of the aldehydes. The appearance of characteristic C=N stretching band (1625 and 1624 cm⁻¹) was observed, thus indicating the formation of imine linkages (Figure S1). The ¹³C cross-polarization magic-angle spinning (CP/MAS) NMR signals of CCOF can be explicitly assigned as the proposed structure. Specifically, the typical signals at about 160 ppm indicated the successful formation of imine bonds for CCOFs **15** and **16** (Figure S2). Circular dichroism (CD) spectra of CCOFs **15** and **16** made from *R* and *S* enantiomers of BINOL monomers are mirror images of each other, which is indicative of their enantiomeric nature (Figure S3). Thermal gravimetric analysis (TGA) reveals that both COFs start to decompose at around 400 °C (Figure S4). Scanning electron microscopy (SEM) images showed CCOF **15** possesses a rod-like morphology with an average particle size of 2 μm while CCOF **16** possesses a slake shaped crystals with an average particle size of 2 μm × 3 μm (Figure S5).

The crystal structures of CCOFs **15** and **16** were determined by powder X-ray diffraction (PXRD) analysis with Cu Kα radiation in conjunction with structural simulations (Figure 1). Referring to the previous report and considering the chiral structure of these COFs, we have simulated several different structures based on the reticular chemistry. After the geometrical energy minimization by using the Materials Studio software package, the detailed simulation (Figures S8 and S9) suggested that CCOFs **15** and **16** were proposed to adopt a 9-fold and 11-fold interpenetrated **dia** topology with the chiral *I*₄ space group, respectively. Full profile pattern matching Pawley refinements for the CCOFs were carried out and the refinement results yield unit cell parameters that are nearly equivalent to the predictions with good agreement factors ($a = b = 30.97$ Å, $c = 7.57$ Å, $\alpha = \beta = \gamma = 90^\circ$, $R_{wp} = 2.51\%$, and $R_p = 1.88\%$ for **15**; $a = b = 37.58$ Å, $c = 7.15$ Å, $\alpha = \beta = \gamma = 90^\circ$, $R_{wp} = 2.64\%$, and $R_p = 1.94\%$ for **16**).

CCOF **15** shows high crystallinity, exhibiting the first intense peak at a low angle 5.70° (2θ), which corresponds to the (200) reflection plane, along with minor peaks at 8.08°, 9.04°, 11.45°, 12.80°, 15.63°, 17.20°, 18.54°, 19.37°, 21.79°, and 22.54°,

attributed to the (220), (130), (400), (240), (321), (600), (341), (521), (451) and (361) reflection planes, respectively. For **16**, the first and most intense peak corresponding to the (200) reflection plane appears at 4.71°, with other minor peaks at 3.33°, 4.75°, 6.66°, 7.45°, 9.40°, 17.74°, 19.02°, and 20.12°, attributed to the (110), (200), (220), (310), (400), (521), (611) and (631) reflection planes, respectively. Notably, some peaks after $2\theta > 10^\circ$ in **15** were violent, while those of **16** showed low intensity, revealing the impact of different linear linkers on the crystalline frameworks.

Also, PXRD patterns were calculated for the two COFs on the other structures, but all of the calculated patterns did not match the experimental patterns well (Figure S8 and S9). CCOFs **15** and **16** are thus proposed to have the architectures shown in Figure 3. The BINOL units in combination with **TAM** induced the formation of a diamond network with 1D open channels of 0.82 nm/1.05 nm for **15** and 1.20 nm/1.52 nm for **16**, respectively. The porosity and surface areas were measured by N₂ adsorption and desorption analysis at 77 K (Figure 1c, d). Both CCOFs show a sharp uptake at a low pressure of $P/P_0 < 0.05$, indicative of their microporous nature. The Brunauer-Emmett-Teller (BET) surface areas were calculated to be 631 and 825 m² g⁻¹ for **15** and **16**, respectively, and the total pore volumes were 0.51 cm³ g⁻¹ and 0.53 cm³ g⁻¹ at $P/P_0 = 0.99$. The pore size distribution analysis were calculated by using the nonlocal density functional theory (NLDFIT) to give rise to a mean pore width 8 Å, 11 Å for **15** and 12 Å, 15 Å for **16**, which are in good agreement with those of the proposed models (Figure 1c and 1d).

The chemical stability of the CCOFs was examined by PXRD and N₂ sorption isotherms after one day of treatment in boiling water, HCl (aqueous), and NaOH (aqueous). The experiment shows that both CCOFs were stable in boiling water and maintained good crystallinity with a small decrease in decreased surface areas compared to the pristine samples (Figures S6 and S7). It was found that CCOF **15** was stable in 0.1 M HCl (aqueous) and 0.1 M NaOH (aqueous), whereas **16** was stable in 0.01 M HCl (aqueous) and 0.01 M NaOH (aqueous), though a small decrease in the signal-to-noise ratio of the PXRD peaks and a little bit decrease of surface areas was observed (Figures S6 and S7). So, CCOF **15** showed improved alkali resistance and antihydrolysis capability relative to **16**, consistent with that the shorter building block could guarantee the rigidity of the framework better.^[20]

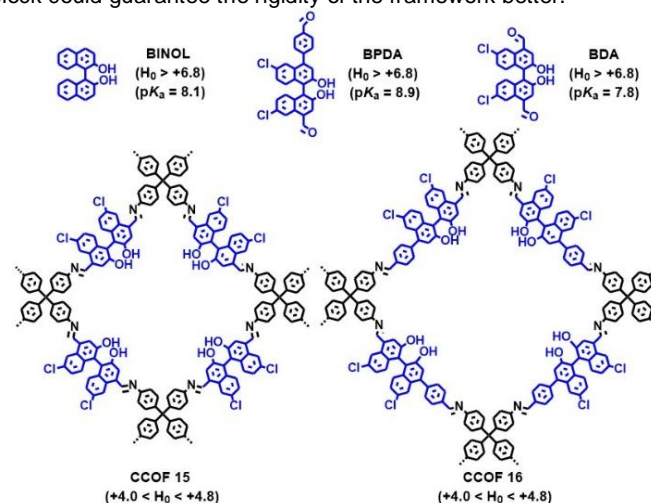


Figure 2. The acidities of the CCOFs and related BINOL acids that are determined by the Hammett indicator method or UV-vis spectrophotometric titration method.

RESEARCH ARTICLE

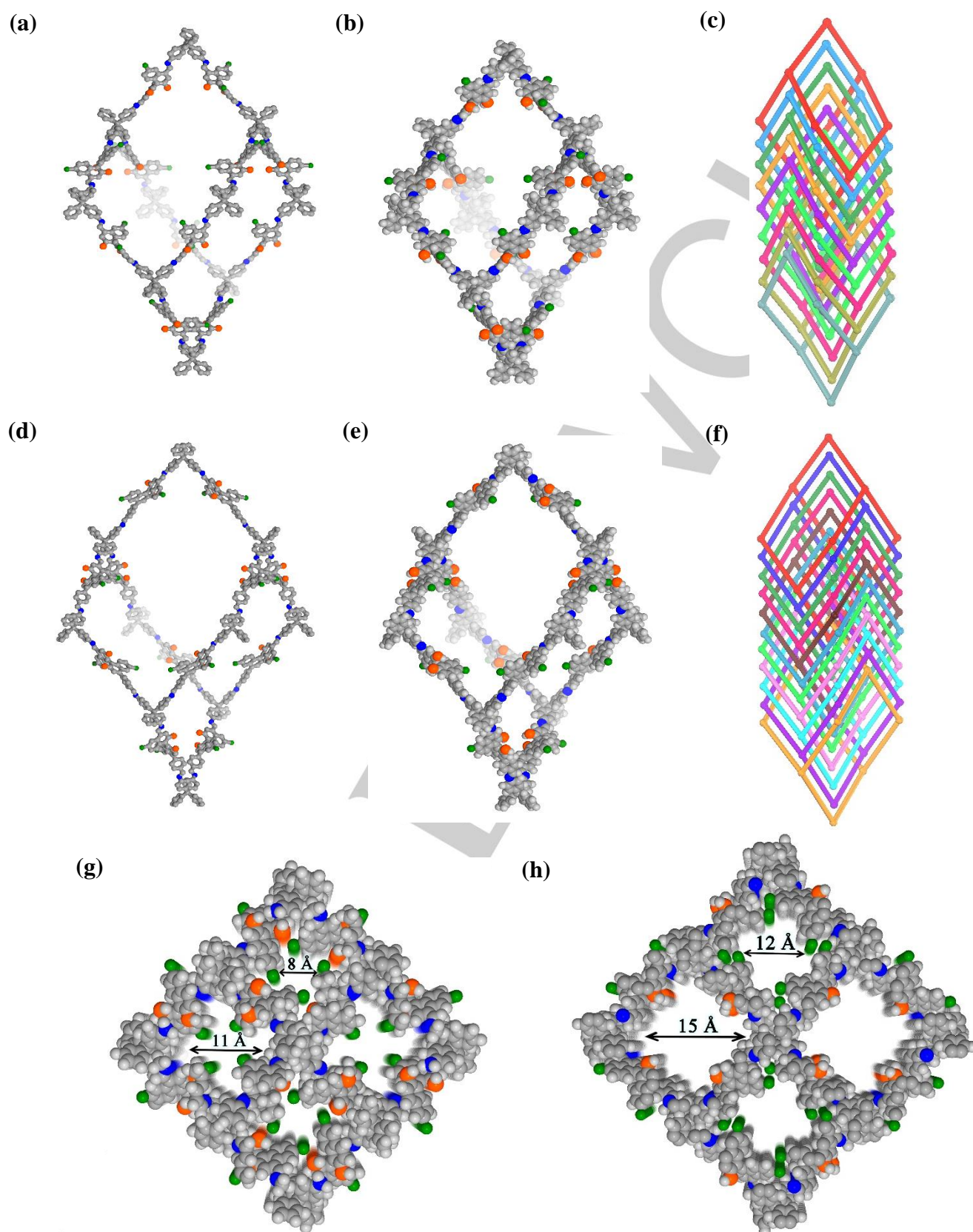


Figure 3. Structural representations of the two COFs. a, b) An adamantane-like cage in CCOF **15** and its space-filling model. d, e) An adamantane-like cage in CCOF **16** and its space-filling model. c, f) Interpenetration of nine and eleven diamond nets in **15** and **16**. g, h) The 3D structure of CCOFs **15** and **16** viewed along the c-axis. C gray; N blue; Cl green; H white; O red.

RESEARCH ARTICLE

Table 1. Asymmetric Acetalization of 2-Aminobenzamide and Aldehydes^a

entry	cat.	R	yield(%) ^b	ee (%) ^c	entry	cat.	R	yield(%)	ee (%)
1	<i>R</i> -15	Ph	89	94	21	<i>R</i> -BDN ^e	Ph	93	0
2		4-FPh	90	96	22		4-FPh	92	0
3		4-ClPh	91	97	23		4-ClPh	94	0
4		4-BrPh	92	94	24		4-BrPh	92	0
5		4-CNPh	80	87	25		4-CNPh	88	0
6		4-OMePh	88	71	26		4-OMePh	90	0
7		4-MePh	81	75	27		4-MePh	93	0
8		4-EtPh	85	76	28		4-EtPh	91	0
9		2-naphthyl	89	95	29		2-naphthyl	91	0
10		G ₁ ^d	55	16	30		G ₁	78	0
11		G ₂	61	0	31		G ₂	87	0
12		G ₃	64	0	32		G ₃	82	0
13		G ₄	<5	n.d.	33		G ₄	85	0
14	<i>R</i> -16	Ph	65	-11	34	<i>R</i> -BPDN ^e	Ph	0	n.d.
15		2-naphthyl	51	-82	35		2-naphthyl	0	n.d.
16		G ₂	79	-41	36		G ₂	0	n.d.
17		G ₃	48	0	37		G ₃	0	n.d.
18	<i>R</i> -BDA	Ph	90	0	38	<i>R</i> -BINOL	Ph	92	0
19		4-FPh	93	0	39		4-FPh	95	0
20		4-OMePh	88	0	40		4-OMePh	90	0

^aReaction conditions: 2-aminobenzamides (0.1 mmol), aldehyde (0.12 mmol), catalyst (COF: 10 mol %, homogeneous catalyst: 10 mol%), MgSO₄ (100 mg, dehydrating agent), CH₃CN (1.0 mL), 40 °C, 24 h. ^bIsolated yield. ^cDetermined by HPLC. ^dG₁ = 1-pyreneyl, G₂ = 9-phenanthrene, G₃ = 4-anthracylphenyl, G₄ = 3,5-bis(3,5-di-*tert*-butylbenzyloxy)phenyl. ^eBDN and BPDN are derivatives of BDA and BPDA, respectively, whose aldehyde groups were protected with neopentylglycol.

The Brønsted acidity of a catalyst is of significant importance for catalytic performances, and so we measured the Brønsted acidity of CCOFs and related BINOL acids by the Hammett indicator method.^[21a] Also, the Brønsted acidity of BINOL monomers was measured in CH₃CN by UV-vis spectrophotometric titration method.^[21b] As shown in Figure 2, all monomers **BDA**, **BINOL**, and **BPDA** have weak acidity, with $H_0 > 6.8$ and pK_a values of 7.8, 8.1, and 8.9, respectively. The order of acidity for three monomers is consistent with the installation of different electron-withdrawing groups on BINOL skeleton. After incorporating into COFs, the acidity of BINOL derivatives was obviously enhanced ($4.0 \leq H_0 \leq 4.8$ for both). The enhanced acidity may be ascribed to condensations of aldehyde groups of the BINOL linkers to amine groups of **TAM**, which can facilitate electrons delocalize over a conjugated structure and prevent the isolated BINOL hydroxyl groups forming intermolecular hydrogen bonding and promoting proton transfer.^[22] Further research is underway to better understand the origin of the enhanced Brønsted acidity of COFs.

Inspired by the highly crystalline nature and accessible pores of the two CCOFs, as well as the chiral channels and the rich hydroxyl protons active sites in frameworks, we have evaluated their heterogeneous catalytic properties in the asymmetric acetalization of 2-aminobenzamides with aldehydes, which is the highly effective method for the synthesis of optically pure 2,3-dihydroquinazolinone (DHQZ).^[18,22] As a privileged scaffold, the DHQZ family of compounds are of critical importance for

pharmacological activities such as antibiotic, antidefibrillatory, vasodilatory and analgesic efficacy.

After screening various reaction conditions including catalyst loading, reaction time, solvent, and temperature (Table S3), we found that CCOF **15** can be an active catalyst for the condensation and cyclization of 2-aminobenzamide with aldehydes. Especially, 10 mol% loading of the COF catalyzed the condensation/amine addition of 4-chloro-benzaldehyde to produce the desired molecule with 91% yield and 97% ee in CH₃CN at 40 °C after 24 h (Table 1, entry 3). Under the optimized conditions, we used other benzaldehyde derivatives to extend the substrate scope. As shown in Table 1, all examined reactions reached completion within 24 h and gave corresponding DHQZ products in good to excellent enantioselectivities (71-97% ee) and 80-92% yields. It was shown that benzaldehydes bearing electron-withdrawing groups with 2-aminobenzamide afforded the DHQZ products in higher yields and ee values than the ones with electron-rich substituents (Table 1, entries 2-8). In sharp contrast, despite the isostructural porous structure, CCOF **16** exhibited much lower enantioselectivity than CCOF **15** in promoting the same reactions, presumably due to the larger channels that has weaker enantioselective induction ability (Table 1, entries 14-15). It is worth noting that the main product configuration catalyzed by (*R*)-**16** is opposite to the product catalyzed by (*R*)-**15**, consistent with that the porous structures of solid catalysts play an important role in the configuration of products.^[23a] The enantioselectivity

RESEARCH ARTICLE

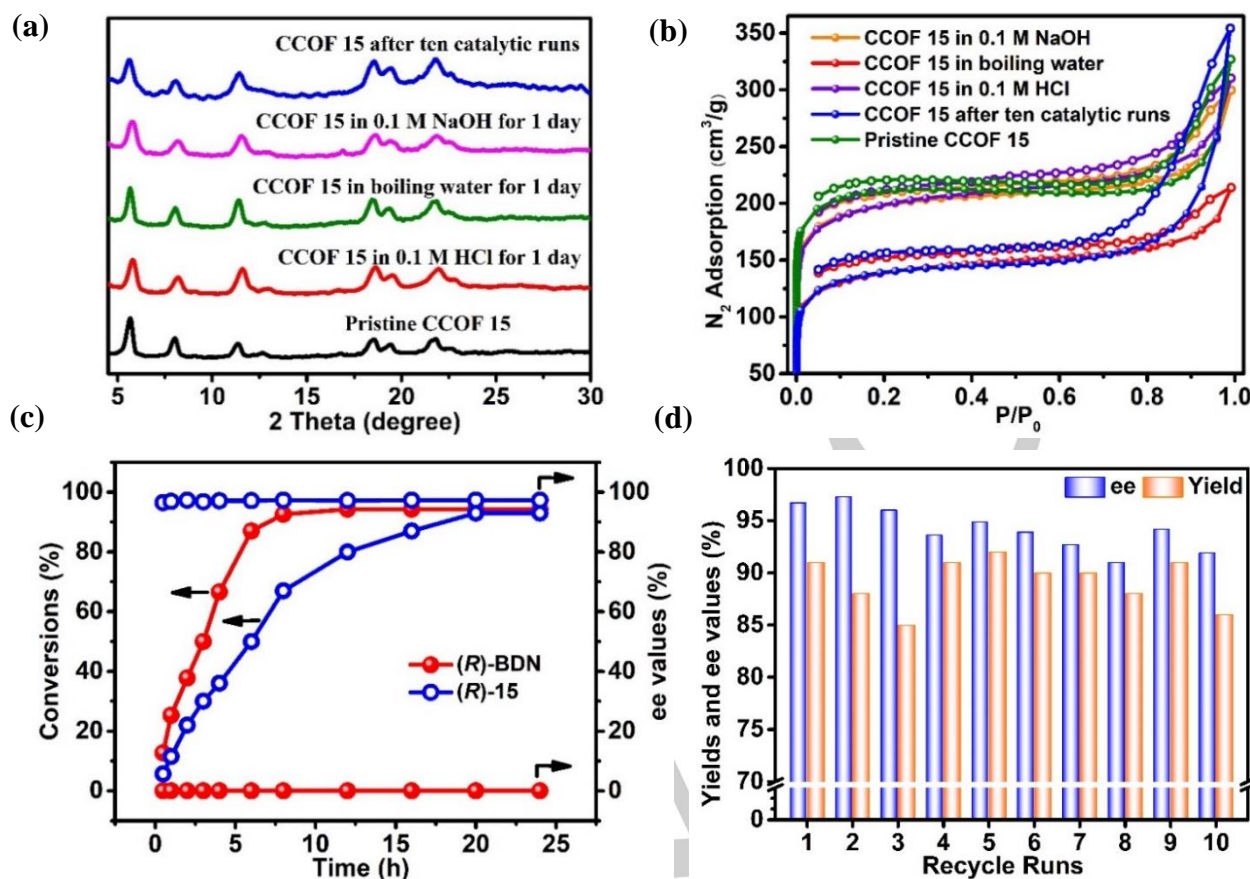


Figure 4. a) PXRD patterns b) N₂ adsorption-desorption isotherms of CCOF 15 upon treatment in different conditions. c) Plots of ee values and conversions with 10 mol % CCOF 15 and of BDN. d) Recycling results of CCOF 15 in the acetalization of 2-aminobenzamides with 4-chlorobenzaldehyde.

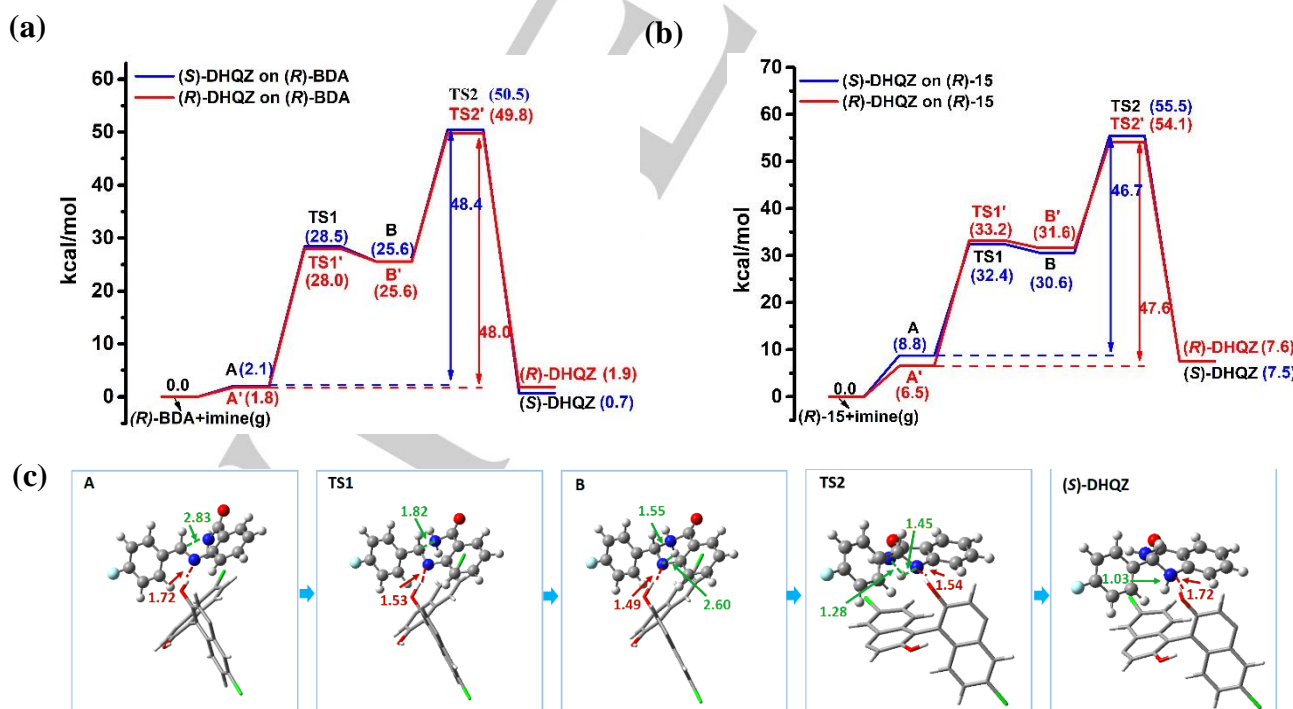


Figure 5. Relative Gibbs energy profiles at 40 °C for the intramolecular amidation of imine to (S)- and (R)-DHQZ on a) (R)-BDA and b) (R)-CCOF 15. c) Simplified structures for (S)-DHQZ production on (R)-BDA. The breaking/forming bonds are labelled in orange, and the hydrogen bonds in red (bond lengths in Å). A/A': imine in adsorbed state; TS1/TS1': transition state for nucleophilic attack of the N atom of amide group on imine C; B/B': cyclization intermediate; TS2/TS2': transition state for H shift from NH₂ to N; (S)/(R)-DHQZ in adsorbed state. C: grey, H: white, O: red, N: blue, F: light blue and Cl: green.

RESEARCH ARTICLE

reversal may result from the chiral environment of the (*R*)-**16** channel, similar to enzymatic catalysis in which the product selectivity is controlled by the enzyme pocket.^[24]

The different catalytic performances of the CCOFs and related homogeneous catalysts were investigated. To eliminate the influence of aldehydes on the catalytic reaction, monomers **BDP** and **BPDP** were converted into **BDN** and **BPDN** by protected their aldehyde groups with neopentylglycol. As shown in Table 1 (entries 21-29), with 10.0 mol% loading of **BDN** (the same loading of BINOL as the COF catalyst), the reaction of anthranilamide with seven different aromatic aldehydes proceeded smoothly, affording the targeted products in 88-94% yields, but with no enantioselectivity in all cases. However, when **BPDN** was used as a catalyst, the reactions cannot take place at all, even with prolonged reaction times (48 h). This is probably due to its extremely weak acidity ($pK_a = 8.9$) that cannot activate the substrates. An in-depth investigation of the reason is still underway. Control experiments showed that pure BINOL exhibited similar catalytic performance to **BDN** in promoting the above reactions (Table 1, entries 38-40). As mentioned above, the presence of catalytic amount of CCOFs can afford the desired chiral DHQZ in high yield and enantioselectivity for CCOF **15** and moderate yield and enantioselectivity for CCOF **16**. Thus, these findings suggested that the porous frameworks containing special chiral cavities constructed from chiral BINOL-derived monomers and **TAM** are essential for enantioselective generation of chiral DHQZ, while the homogenous catalysts are incapable of providing stereocontrol on the products. Moreover, incorporation of **BPDA** units into the COF can obviously enhance the Brønsted acidity and endow them with catalytic activity.

To further understand the catalytic process of the COF and homogeneous control, we monitored the dynamic process in the synthesis of 2-(4-chlorophenyl)-2,3-DHQZ by CCOF **15** or **BDN**. As shown in Figure 4c, the transformations displayed different reaction kinetics. The reactions catalyzed by CCOF **15** and **BDN** were completed in 12 h and 20 h, respectively. In particular, the ee values of the products were around 97% from the beginning to the end for CCOF **15**, and the values were always 0% for **BDN**. The COF-catalyzed reactions needed longer time can be ascribed to slow mass diffusion in the porous solid catalyst.

Recycle experiments were conducted to examine the heterogeneity and recyclability of the COF catalyst. Upon completion of the catalytic reaction, CCOF **15** could be recovered by centrifugation and reused at least for ten times without any obvious loss of its activity and enantioselectivity (Figure 4d). The PXRD pattern and N₂ absorption and desorption isotherms showed that CCOF **15** remained its crystallinity and porosity after ten catalytic recycles, though there was a slightly decreased signal-to-noise ratio and a little bit decrease of surface areas (436 m²g⁻¹), as shown in Figures 4a and 4b.

To study the role of the CCOF channels in catalysis, several aromatic aldehydes with different sizes were selected and subjected to the reactions. As illustrated in Table 1, the **BDN** promoted condensation and cyclization of 2-aminobenzamide with the bulky aldehydes to produce DHQZ in high yields (Table 1, entries 30-33). In contrast, the yields of the reaction products catalyzed by CCOF **15** gradually decreases when the sizes of the aldehyde substrates increases (Table 1, entries 10-13). When 9-phenanthrenecarbaldehyde, which has the size (9 Å × 11 Å) between the channel diameters of CCOFs **15** and **16**, was

subjected to the reaction, **15** afforded the targeted product in 61% yield, lower than the 79% yield obtained with **16**. Furthermore, for the more bulky substrate 3,5-bis(3,5-di-tert-butyl)benzyloxybenzaldehyde (14 × 21 Å²), only trace yield of the product was detected catalyzed by CCOF **15**, which was much lower than the 85% yield obtained with **BDN**. This very low yield is probably attribute to that the very bulky substrate cannot access the catalytically active Brønsted acid sites in the CCOF cavity through the windows (8 × 11 Å²) because of its large diameter. Taken together, the above results indicate that the reaction mainly occurs inside the pores.

To rationalize the difference in the enantioselectivity of DHQZ observed experimentally, we performed density functional theory (DFT) calculations for the reaction catalyzed by (*R*)-**BDA** and (*R*)-**15** (Figures S17 and S18), respectively. Previous studies have suggested the enantioselectivity of DHQZ is determined by the intramolecular amidation of imine,^[18] which is also the focus in our calculations. The DFT calculations illustrated in Figures S18 and S19 indicate the intramolecular amidation of imine consists of two steps. A cyclization intermediate is firstly generated through nucleophilic attack of the N atom of amide group on imine C, and then DHQZ is produced along with H shift from NH₂ to N. For intramolecular amidation of imine on (*R*)-**BDA** (it was assumed that the aldehyde groups of **BDA** did not involve the reactions), the imine interacts with (*R*)-**BDA** through hydrogen bond between the N atom of the reactant and the hydroxyl group of (*R*)-**BDA**, in addition to π-π interaction. As shown in Figure 5a, the overall barriers are predicted to be 48.4 and 48.0 kcal/mol for (*S*)- and (*R*)-DHQZ, respectively, which indicates a rather low enantioselectivity. For intramolecular amidation of imine on (*R*)-**15** (Figures S20 and S21), the imine is located in the channel and interacts with (*R*)-**15** also through hydrogen bond. The overall barriers for (*S*)- and (*R*)-DHQZ production are computed to be 46.7 and 47.6 kcal/mol, respectively (Figure 5b). Since the barrier difference on (*R*)-**15** (0.9 kcal/mol) is obviously larger than that on (*R*)-**BDA** (0.4 kcal/mol), a higher enantioselectivity thus can be expected on (*R*)-**15**. This is qualitatively consistent with the experimental observed trend. Therefore, the confinement effect in (*R*)-**15** makes intramolecular amidation of imine *via* Si face more favourable, which is responsible for the preferential production of (*S*)-DHQZ in (*R*)-**15**.

A variety of chiral solid Brønsted acids including solid phosphoric acid have been explored as heterogeneous catalysts for the enantioselective synthesis of 2,3-dihydroquinazolinone,^[22,25] but in most cases, only moderate to excellent enantioselectivities were observed.^[25c] Diol organocatalysts typically cannot enantioselectively catalyzing acetalization reactions of 2-aminobenzamide and aldehydes.^[18] Remarkably, the present 3D COFs enable the nonselective chiral BINOL to enantioselectively catalyze the acetalization of 2-aminobenzamides and aldehydes to produce enantiomeric purity DHQZ. The ee values of this COF-based protocol are higher or comparable well to those of the enantioselective MOF-phosphoric acid heterogeneous catalysts^[18,22] and even homogeneous phosphoric acid catalysts,^[19] as summarized in Table S4. To the best of our knowledge, this is the first report on utilization of the COF platform to boost a homogeneous catalyst from completely nonselective to highly selective.^[18] Further research on using the CCOF catalysts with different types of acid-active sites for more important and challenging catalytic reactions is in progress.

RESEARCH ARTICLE

Conclusion

We have reported two 3D CCOFs with interpenetrated open frameworks that were prepared by imine condensation of tetrahedral tetraamine and chiral BINOL dialdehydes. The BINOL hydroxyl groups that are periodically aligned within the tubular channels exhibit greatly enhanced acidity relative to the free acids and can function as heterogeneous Brønsted acid catalysts for the asymmetric acetalization of aromatic aldehydes and 2-aminobenzamide to generate the products with up to 93% yield and 97% ee. In contrast, the corresponding homogeneous controls display no enantioselectivity. The COFs catalysts display high robustness and can be recycled multiple times without deterioration of catalytic activity and enantioselectivity. DFT calculations suggest that the induced enantioselectivity of BINOL can be ascribed to the steric hindrance and confinement effect of framework. By enantioselective induction under confinement, we can expect that more novel heterogeneous asymmetric catalysts can be designed and constructed from non-enantioselective catalysts.

Acknowledgements

The authors acknowledge the financial support of the National Science Foundation of China (Grant Nos. 21620102001, 91856204, 91956124 and 21875136), the National Key Basic Research Program of China (2016YFA0203400), Key Project of Basic Research of Shanghai (19JC1412600, 17JC1403100 and 18JC1413200), and Shanghai Rising-Star Program (19QA1404300), the China Postdoctoral Innovative Talent Support Program (BX20190195) and the China postdoctoral science foundation (2019M661483).

Conflict of interest

The authors declare no conflict of interest.

Keywords: covalent organic framework • porosity • catalysis • chirality • crystal engineering

- [1] a) R. Noyori, I. Tomino, Y. Tanimoto, *J. Am. Chem. Soc.* **1979**, *101*, 3129; b) R. Noyori, I. Tomino, Y. Tanimoto, M. Nishizawa, *J. Am. Chem. Soc.* **1979**, *101*, 5843; c) J. M. Brunel, *Chem. Rev.* **2005**, *105*, 857.
- [2] a) B. D. Chapsal, Z. Hua, I. Ojima, *Tetrahedron-Asymmetry* **2006**, *17*, 642; b) K. Yasumoto, T. Kano, K. J. Maruoka, *Org. Chem.* **2020**, *85*, 10232; c) Y. Liu, I. D. Gridnev, W. Zhang, *Angew. Chem., Int. Ed.* **2014**, *53*, 1901.
- [3] a) L. Pu, *Acc. Chem. Res.* **2012**, *45*, 150; b) H. L. Liu, H. P. Zhu, X. L. Hou, L. Pu, *Org. Lett.* **2010**, *12*, 4172.
- [4] a) S. Zhang, Y. Wang, F. Meng, C. Dai, Y. Cheng, C. Zhu, *Chem. Commun.* **2015**, *51*, 9014; b) H. Maeda, Y. Bando, K. Shimomura, I. Yamada, M. Naito, K. Nobusawa, H. Tsumatori, T. Kawai, *J. Am. Chem. Soc.* **2011**, *133*, 9266.
- [5] a) Y. Chen, S. Yekta, A. K. Yudin, *Chem. Rev.* **2003**, *103*, 3155; b) R. Alam, C. Diner, S. Jonker, L. Eriksson, K. J. Szabó, *Angew. Chem. Int. Ed.* **2016**, *55*, 14417.
- [6] a) K. Matsui, S. Takizawa, H. Sasai, *J. Am. Chem. Soc.* **2005**, *127*, 3680; b) J. M. Wieting, T. J. Fisher, A. G. Schafer, M. D. Visco, J. C. Gallucci, A. E. Mattson, *Eur. J. Org. Chem.* **2015**, *2015*, 525; c) Y. Zhang, N. Li, B. Qu, S. Ma, H. Lee, N. C. Gonnella, J. Wang, *Org. Lett.* **2013**, *15*, 1710.
- [7] a) W. Y. Han, J. Zuo, X. M. Zhang, W. C. Yuan, *Tetrahedron* **2013**, *69*, 537; b) L. Bayeh, P. Q. Le, U. K. Tambar, *Nature* **2017**, *547*, 196.
- [8] D. J. Gorin, B. D. Sherry, F. D. Toste, *Chem. Rev.* **2008**, *108*, 3351.
- [9] a) A. P. Côté, A. I. Benin, N. W. Ockwig, M. O'keeffe, A. J. Matzger, O. M. Yaghi, *Science* **2005**, *310*, 1166; b) C. S. Diercks, O. M. Yaghi, *Science* **2015**, *355*, 6328.
- [10] a) S. Y. Ding, W. Wang, *Chem. Soc. Rev.* **2013**, *42*, 548; b) T. Ma, E. A. Kapustin, S. X. Yin, L. Liang, Z. Zhou, J. Niu, X. Wang, *Science* **2018**, *361*, 48; c) X. Han, C. Yuan, B. Hou, L. Liu, H. Li, Y. Liu, Y. Cui, *Chem. Soc. Rev.* **2020**, *49*, 6248; d) J. Dong, X. Han, Y. Liu, H. Li, Y. Cui, *Angew. Chem. Int. Ed.* **2020**, *59*, 13722.
- [11] a) H. Furukawa, O. M. Yaghi, *J. Am. Chem. Soc.* **2009**, *131*, 8875; b) H. Fan, A. Mundstock, A. Feldhoff, A. Knebel, J. Gu, H. Meng, J. Caro, *J. Am. Chem. Soc.* **2018**, *140*, 10094; c) P. Das, S. K. Mandal, *Chem. Mater.* **2019**, *31*, 1584; d) J. Huang, X. Han, S. Yang, Y. Cao, C. Yuan, Y. Liu, J. Wang, Y. Cui, *J. Am. Chem. Soc.* **2019**, *141*, 8996.
- [12] a) S. DALapati, S. Jin, J. Gao, Y. Xu, A. Nagai, D. Jiang, *J. Am. Chem. Soc.* **2013**, *135*, 17310; b) G. Lin, H. Ding, D. Yuan, B. Wang, C. Wang, *J. Am. Chem. Soc.* **2016**, *138*, 3302; c) S. Y. Ding, M. Dong, Y. W. Wang, Y. T. Chen, H. Z. Wang, C. Y. Su, W. Wang, *J. Am. Chem. Soc.* **2016**, *138*, 3031; d) L. Ascherl, E. W. Evans, J. Gorman, S. Orsborne, D. Bessinger, T. Bein, R. H. Friend, F. Auras, *J. Am. Chem. Soc.* **2019**, *141*, 15693; e) S. Jhulki, A. M. Evans, X. L. Hao, M. W. Cooper, C. H. Feriante, J. Leisen, H. Li, D. Lam, M. C. Hersam, S. Barlow, J. L. Brédas, W. R. Dichtel, S. R. Marder, *J. Am. Chem. Soc.* **2020**, *142*, 783.
- [13] a) S. Y. Ding, J. Gao, Q. Wang, Y. Zhang, W. G. Song, C. Y. Su, W. Wang, *J. Am. Chem. Soc.* **2011**, *133*, 19816; b) W. Chen, Y. Tang, B. Aguila, Y. Pan, A. Zheng, Z. Yang, L. Wojtas, S. Ma, F. S. Xiao, *Matter* **2020**, *2*, 416; c) Y. Wan, L. Wang, H. Xu, X. Wu, J. Yang, *J. Am. Chem. Soc.* **2020**, *142*, 4508; d) S. Lu, Y. Hu, S. Wan, R. McCaffrey, Y. Jin, H. Gu, W. Zhang, *J. Am. Chem. Soc.* **2017**, *139*, 17082; e) X. Wang, L. Chen, S. Y. Chong, M. A. Little, Y. Wu, W. H. Zhu, R. Clowes, Y. Yan, M. A. Zwiijnenburg, R. S. Sprick, A. I. Cooper, *Nat. Chem.* **2018**, *10*, 1180; f) X. Wu, X. Han, Y. Liu, Y. Cui, *J. Am. Chem. Soc.* **2018**, *140*, 16124; g) X. Kang, X. Han, C. Yuan, C. Cheng, Y. Liu, Y. Cui, *J. Am. Chem. Soc.* **2020**, *142*, 16346; h) X. Han, Q. Xia, J. Huang, Y. Liu, C. Tan, Y. Cui, *J. Am. Chem. Soc.* **2017**, *139*, 8693.
- [14] a) Q. Fang, J. Wang, S. Gu, R. B. Kaspar, Z. Zhuang, J. Zheng, H. Guo, S. Qiu, Y. Yan, *J. Am. Chem. Soc.* **2015**, *137*, 8352; b) S. Bhunia, K. A. Deo, A. K. Gahawar, *Adv. Funct. Mater.* **2020**, *30*, 2002046; c) C. Wang, H. Liu, S. Liu, Z. Wang, J. Zhang, *Front. Chem.* **2020**, *8*, 488.
- [15] a) H. L. Qian, C. X. Yang, X. P. Yan, *Nat. Commun.* **2016**, *7*, 12104; b) X. Han, J. Huang, C. Yuan, Y. Liu, Y. Cui, *J. Am. Chem. Soc.* **2018**, *140*, 892; c) C. Yuan, X. Wu, R. Gao, X. Han, Y. Liu, Y. Long, Y. Cui, *J. Am. Chem. Soc.* **2019**, *141*, 20187.
- [16] X. Wu, X. Han, Q. Xu, Y. Liu, C. Yuan, S. Yang, Y. Liu, J. Jiang, Y. Cui, *J. Am. Chem. Soc.* **2019**, *141*, 7081.
- [17] a) H. Xu, J. Gao, D. Jiang, *Nat. Chem.* **2015**, *7*, 905; b) H. Xu, S. Ding, W. An, H. Wu, W. Wang, *J. Am. Chem. Soc.* **2016**, *138*, 11489; c) X. Wang, X. Han, J. Zhang, X. Wu, Y. Liu, Y. Cui, *J. Am. Chem. Soc.* **2016**, *138*, 12332; d) J. Zhang, X. Han, X. Wu, Y. Liu, Y. Cui, *J. Am. Chem. Soc.* **2017**, *139*, 8277; e) S. Zhang, Y. Zheng, H. An, B. Aguila, C. X. Yang, Y. Dong, W. Xie, P. Cheng, Z. Zhang, Y. Chen, S. Ma, *Angew. Chem. Int. Ed.* **2018**, *57*, 16754; f) H. C. Ma, C. C. Zhao, G. J. Chen, Y. B. Dong, *Nat. Commun.* **2019**, *10*, 3368; g) L. K. Wang, J. J. Zhou, Y. B. Lan, S. Y. Ding, W. Yu, W. Wang, *Angew. Chem. Int. Ed.* **2019**, *58*, 9443.
- [18] C. Tan, K. Yang, J. Dong, Y. Liu, J. Jiang, Y. Cui, *J. Am. Chem. Soc.* **2019**, *141*, 17685.
- [19] a) D. Huang, X. Li, F. Xu, L. Li, X. Lin, *ACS Catal.* **2013**, *3*, 2244; b) X. Cheng, S. Vellalath, R. Goddard, B. List, *J. Am. Chem. Soc.* **2008**, *130*, 15786.
- [20] C. Qian, Q. Y. Qi, G. F. Jiang, F. Z. Cui, Y. Tian, X. Zhao, *J. Am. Chem. Soc.* **2017**, *139*, 6736.
- [21] a) C. Walling, *J. Am. Chem. Soc.* **1950**, *72*, 1164; b) K. Kaupmees, N. Tolstoluzhsky, S. Raja, M. Rueping, I. Leito, *Angew. Chem. Int. Ed.* **2013**, *52*, 11569.
- [22] a) W. Gong, X. Chen, H. Jiang, D. Chu, Y. Cui, Y. Liu, *J. Am. Chem. Soc.* **2019**, *141*, 7498; b) X. Chen, H. Jiang, X. Li, B. Hou, W. Gong, X. Wu, X.

RESEARCH ARTICLE

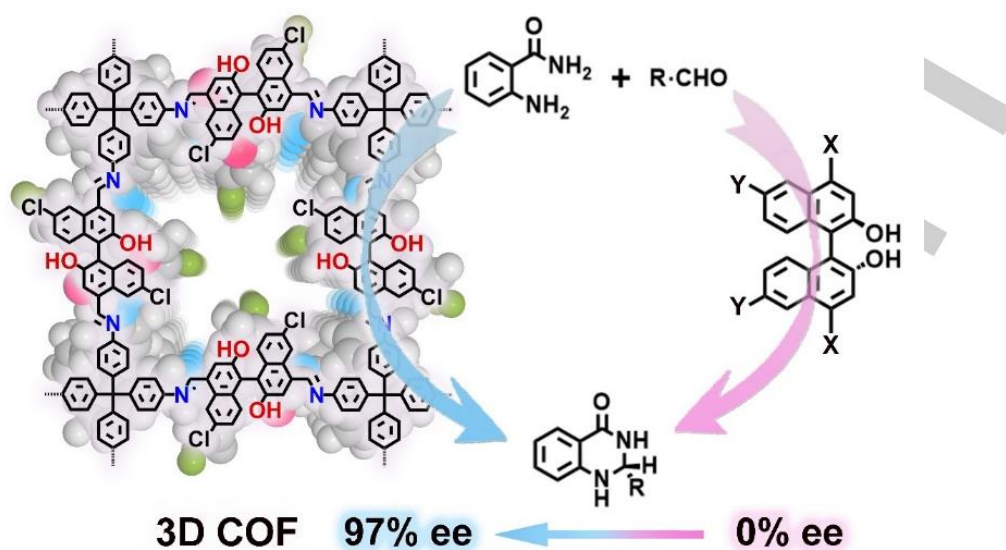
- Han, F. Zheng, Y. Liu, J. Jiang, Y. Cui, *Angew. Chem. Int. Ed.* **2019**, *58*, 14748.
- [23] a) M. Zheng, Y. Liu, C. Wang, S. Liu, W. Lin, *Chem. Sci.* **2012**, *3*, 2623; b) H. Jiang, W. Zhang, X. Kang, Z. Cao, X. Chen, Y. Liu, Y. Cui, *J. Am. Chem. Soc.* **2020**, *142*, 9642.
- [24] (a) A. J. Kirby, *Angew. Chem., Int. Ed.*, **1996**, *35*, 706; (c) Y. Murakami, J.-i. Kikuchi, Y. Hisaeda and O. Hayashida, *Chem. Rev.*, **1996**, *96*, 721.
- [25] a) X. Zhang, A. Kormos, J. Zhang, *Org. Lett.* **2017**, *19*, 6072; b) B. Zhang, L. Shi, R. Guo, *Catal. Lett.* **2015**, *145*, 1718; c) C. Monterde, R. Navarro, M. Iglesias, F. Sanchez, *J. Catal.* **2019**, *377*, 609.

WILEY-VCH

Accepted Manuscript

RESEARCH ARTICLE

Entry for the Table of Contents



The chiral 3D COFs with interpenetrated open frameworks were synthesized by condensation of tetrahedral tetraamine and enantiopure 1,1'-binaphthol (BINOL) dialdehydes. The Brønsted acidity of BINOL hydroxyl groups that are periodically aligned within the COFs was enhanced obviously compared to the non-immobilized acids. The resulting 3D COF was capable of inducing chiral molecular catalysts from non-enantioselective to highly enantioselective under confinement effect in catalyzing important organic transformation with high catalytic activity and good recyclability.